# Evidence of climate-driven changes on atmospheric, hydrological, and oceanographic variables along the Chilean coastal zone

Patricio Winckler Grez [1,2,3] (ID) · Catalina Aguirre [1,3,4] · Laura Farías [4,5] · Manuel Contreras-López [6] · Ítalo Masotti [3,4,7]

## Abstract

The Chilean coastal zone (CCZ) is subjected to a complex spectrum of anthropogenic, geophysical, biogeochemical, and climate-driven perturbations. Potentially affected variables including atmospheric sea level pressure ($Pa$), alongshore wind, sea surface temperature ($SST$), chlorophyll-a, rainfall, river discharge, relative mean sea level ($RMSL$), and wave climate are studied using in situ and satellite records, hindcasts, and reanalysis datasets. Linear temporal trends and correlations of anomalies are estimated between 18°S and 55°S along the CCZ. The comparison of some of the variables is achieved by means of a strict homogenization procedure on a monthly basis for 35 years. Our findings show that the poleward drift and strengthening of the Southeast Pacific Subtropical Anticyclone (SPSA) partially explains the increase in $Pa$ and reduction in rainfall and river discharge. The enhancement of alongshore winds, also attributable to changes in the SPSA, increases coastal upwelling, which in turn could reduce $SST$ and increase chlorophyll-a. Despite differential latitudinal responses, increasing wave heights and a southward rotation are evidenced. $RMSL$ does not show significant variation as it is presumably affected by seafloor changes during the seismic cycle. Though some correlations are evidenced, the influence of climate variability at decadal scale (PDO, SAM) may be affecting the detected trends due to the short length of available data. Impacts on coastal communities, infrastructure, and ecosystems are discussed, aiming to highlight that coastal vulnerabilities and risk management should be based on the cumulative impacts of these variables.

✉ Patricio Winckler Grez
patricio.winckler@uv.cl; https://orcid.org/0000–0003–2100–293X

Extended author information available on the last page of the article

# 1 Introduction

Chile has an extensive coastline facing the southeast Pacific Ocean (Fig. 1a). The territory is characterized by strong latitudinal gradients, with a climate ranging from the most arid region worldwide in the north (18°S~30°S), to the rainforests and tundra of the Patagonian fjords (41°~55°S). The country is bounded by the Pacific Ocean to the west and the Andean range to the east, thus creating a marked altitudinal gradient as well. Furthermore, its geomorphology is shaped by the Peru-Chile trench, formed by the subduction of the Nazca Plate beneath South America, which enhances seismic activity. These features provide unique conditions which make the country a natural laboratory to investigate climate trends and coastal hazards. Indeed, between 1980 and 2011, Chile lost nearly 1.2% of its gross domestic product due to natural disasters, a significant part of which is due to meteorological drivers (floods, winds, and storm surges), earthquakes, and tsunamis (UNISDR 2015). Additionally, climate-driven changes have shown negative impacts upon several processes affecting the CCZ, such as coastal erosion, impact on wetlands, and operational downtime of ports (MMA 2019).

Climate-driven changes also have consequences in coastal upwelling occurring in north-central Chile (18°S–38°S), belonging to Eastern Boundary Upwelling Systems (EBUS) which are one of the world's most productive ocean ecosystems, supporting coastal communities and
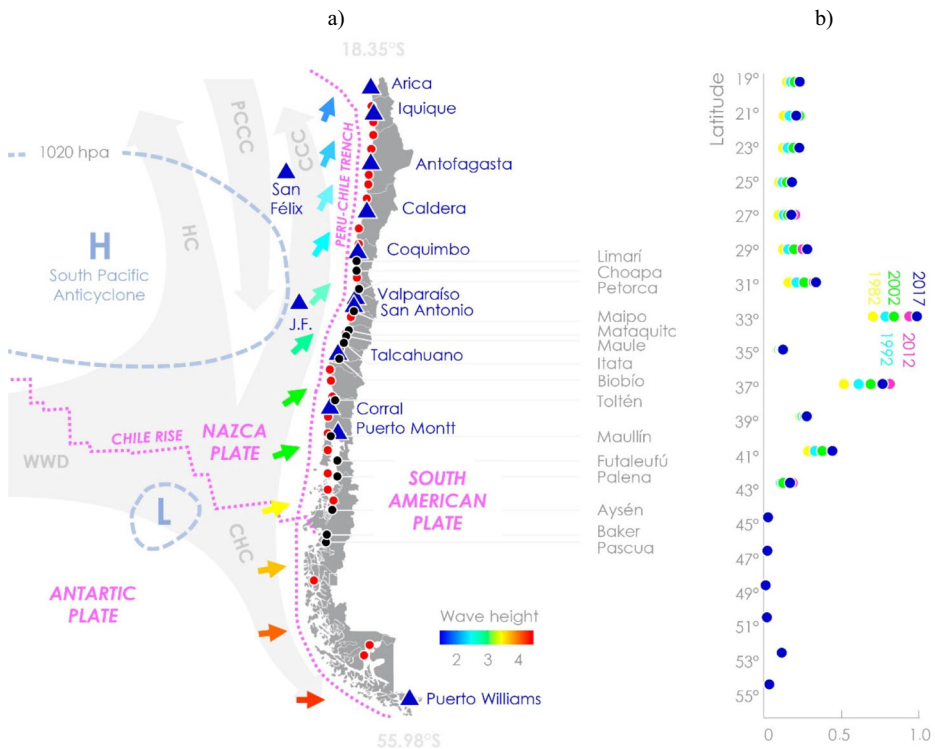


Fig. 1 (a) EBUS (light gray arrows), typical atmospheric pressure pattern (light blue) including the SPSA (*H*) and a extratropical cyclone (*L*), tectonic setting (pink), tide gauges with records of more (blue triangles) or less (red dots) than 30 years, analyzed rivers (black dots), mean annual significant wave height (*Hs*), and wave direction (*Dm*) offshore Chile (in colored arrows), every 2° of latitude (adapted from Beyá et al. 2016). (b) Population of coastal municipalities lumped every 2° of latitude for 5 censuses (INE 2017)

providing benefits to human society (García-Reyes et al. 2015). However, EBUS in a warming word seem to be subject to changes cross-shore atmospheric pressure gradients and intensification in upwelling-favorable wind that may have consequences not yet well evaluated in marine productivity, fisheries, and biogeochemistry (García-Reyes et al. 2015). Based on past records and future projections, studies show that the upwelling-favorable winds over EBUS had and will intensify (e.g., Bonino et al. 2019), although the driving mechanism is still debated. Pauly and Zeller (2016) provide an overview of the likely effects of climate change on EBUS.

To understand climate-driven changes on atmospheric, hydrological, and oceanographic variables, we compute temporal trends and correlations among several variables, e.g., *Pa*, alongshore wind, rainfall, river discharge, *SST*, chlorophyll-a, *RMSL*, and wave climate along the CCZ (18°S–55°S). Our objective is to contribute with scientific evidence by rebuilding long-term time series on coastal processes that will be used in National Adaptation Plans for climate change in fisheries, infrastructure, and coastal zone. Chile is one of the most vulnerable countries to climate change, having seven of the nine characteristics that define a country as vulnerable. Thus, our findings are analyzed from an interdisciplinary viewpoint, reflected on diverse mechanisms and consequences these correlations have on coastal communities, which are particularly vulnerable to processes described by the analyzed variables.

## 2 Study area

Two distinct coastal geomorphological types exist in the CCZ. Between 18.4°S and 41.5°S, there is almost 2600 km of rectilinear coastline comprised by cliffs, dune fields, wetlands, peninsulas, and few bays where major coastal cities and ports are situated. This coastline has one of the narrowest continental shelves worldwide (Paris et al. 2016), seldom interrupted by submarine canyons. In contrast, Patagonia (41.5°S–55.6°S) covers 1700 km of islands and channels, representing one the most extensive fjord region in the world.

The CCZ is characterized by a mosaic of climate types ranging from desert to semi-arid in the north, Mediterranean climate in the central zone, rainforest in the south, and subpolar forests and tundra in Patagonia. Rainfall ranges from almost no precipitation in the desert to more than 4500 mm year$^{-1}$ in the south, while mean annual temperatures range between 18 °C in the north and 5 °C in Patagonia. The main factors controlling the coastal climate are the presence of the SPSA, the Humboldt Current System (Strub et al. 1998), the southern circumpolar current (Talley et al. 2011), and the Andean range (Garreaud 2009). Some of these factors are affected by climate variability in the form El Niño Southern Oscillation (ENSO), the Southern Annular Mode (SAM), and the Pacific Decadal Oscillation (PDO) (e.g., Combes et al. 2009; Ancapichún and Garcés-Vargas 2015; Lara et al. 2016).

The Humboldt Current System (Fig. 1a) is one of the major EBUS and is renowned for prolific pelagic and benthic fisheries and macroalgae (e.g., Thiel et al. 2007; Montecino and Lange 2009). It has several upwelling centers, where salty, cool, oxygen-poor, and nutrient-rich subsurface waters of equatorial origin upwells to the surface as a response to alongshore wind stress on the surface water. This system is among the most productive marine ecosystems worldwide, having an annual net primary production rate of ∼ 1.1 kgC m$^{-2}$ year$^{-1}$ (Testa et al. 2018), enough to sustain sizeable pelagic fisheries (Cubillos et al. 1998). The SPSA influences wind intensity and direction, thus regulating permanent and seasonal coastal upwelling in northern and central Chile. South of 42°, predominately eastward winds are associated with the

westerlies wind belt. Additionally, in this region, surface currents change direction following the bifurcation of the eastward West Wind Drift into the equatorward Humboldt and Chile Coastal currents, and the poleward Cape Horn Currents (Strub et al. 2019, Fig. 1a).

Temporal variability of the SPSA, wind stress, and coastal upwelling off Chile have been well documented over seasonal (Strub et al. 1998), interannual, and decadal scales (e.g., Rahn and Garreaud 2014). Intensification and fluctuation of the SPSA also influences the annual cycle of rainfall in central and southern Chile (Montecinos and Aceituno 2003), thus affecting runoff and river discharge into the coastal zone (Boisier et al. 2018). Consequently, changes in these variables lead to alterations in nutrient and particle export from rivers, thus altering water turbidity and coastal systems function (Masotti et al. 2018).

Wave climate is controlled by swells emerging from extratropical cyclones (Fig. 1a) moving on a latitudinal belt between 40°S and 60°S. The intense winds associated with extratropical cyclones transfer energy to waves, which propagate from the South Pacific Ocean toward the CCZ. Due to Chile's length, strong latitudinal gradients in wave climate range from highly energetic western waves in the south to a relatively mild wave climate in the north (Beyá et al. 2016), due to the greater distance from the wave generation zone (Fig. 1b).

# 3 Data and methods

Data analysis is based on the evaluation of decadal trends and correlations of atmospheric, oceanographic, hydrologic, and biogeochemical variables along the CCZ. $Pa$, alongshore winds at 10 m above sea level ($Ua$), sea surface temperature ($SST$), and rainfall ($r$) are obtained from the ERA-Interim reanalysis (Dee et al. 2011) at 19 numerical points along the coast between 1979 and 2016. $RMSL$ records are analyzed at 11 stations with more than 30 years of data (blue triangles, Fig. 1a). Wave climate is obtained between 1980 and 2015 from an offshore wave hindcast (Beyá et al. 2016) consisting of a time series of 3-h intervals of significant wave height ($Hs$), mean wave period ($Tm$), and mean wave direction ($Dm$) at 19 numerical points off the CCZ. Daily mean discharges are available at 15 fluviometric stations (black dots, Fig. 1a) located in the vicinity of river mouths ($CR^2$ 2019). Chlorophyll-a (phytoplankton biomass) data from SeaWiFS (1997–2002) and MODIS-Aqua (2002–2017) are extracted on an 8-day basis at 19 locations. Finally, nutrient export to the coast (i.e., phosphate and nitrate) is estimated from stations at four rivers in central Chile between 2000 and 2017. Regardless of their original format, all variables are transformed to monthly median values.

Field variables obtained from hindcasts, reanalysis, and satellite data are analyzed every 2° of latitude (19°S–55°S), wherever data dating back to 35 years is available. No gaps are found on these data. Instrumental records ($RMSL$, river discharge, and nutrient export) are subjected to a strict quality control and homogenization in order to generate monthly medians. Gaps are identified and patched wherever possible while poor data is disregarded. Details of data sources, pre and post processing, are provided in the supplementary material.

For each monthly time series, linear trends are estimated using the non-parametric Thiel-Sen estimator (Theil 1950; Sen 1968), a robust method based on the median that remains stable under the presence of outliers (Wilcox 2001). The least square method, on the other hand, is only used to estimate trends for data stemming from the temporal integration of raw data on a monthly level (e.g., rainfall and number of

extreme wave events). To quantify the uncertainty for each point $j$, the 95% interval is obtained by the expression

$$U_j = SE_j \times CV \tag{1}$$

where the critical value $CV$ is obtained from the $t$-Student distribution with $N-2$ degrees of freedom for $N$ years. The standard error is computed as

$$SE_j = \sqrt{\frac{\sum_{i=1}^{N}\left(y_{i,j}-\widehat{y}_{i,j}\right)^2}{(N-2)\sum_{i=1}^{N}\left(t_i-\bar{t}\right)^2}}, \tag{2}$$

where $y_{i,j}$ are the data and $\widehat{y}_{i,j}$ are the estimated values obtained from the linear fit for $N$ years. Linear trends for each variable (Fig. 2 obtained from Figures A1-A8, supplementary material) are then removed from the original time series to obtain the detrended signal. The annual cycle is obtained by averaging out monthly values of the detrended signal throughout the measured/modelled period. The annual cycle is then removed from the detrended signal to obtain the anomaly. Additionally, the anomaly is analyzed in the frequency domain to verify that the annual cycle is properly removed and to identify modes associated to climate variability (supplementary material).

Correlations are computed from anomalies among variables available between 19°S and 55°S for at least 35 years (*Hs*, *Tm*, *Dm*, *Pa*, *SST*, *Ua*; Fig. 3). We arbitrarily assume that variables are correlated when the coefficient of determination is $|R^2| \geq 0.5$, implying that at least 50% of the variance of one variable is explained by a linear regression model with other. When $|R^2| < 0.5$, the correlation is assumed weak. Instrumental records (*RMSL*, *Q*), variables obtained from the monthly temporal integration (*Ne*, *r*), and those with short records (chlorophyll-a) are excluded from this analysis.

In order to highlight the impact of changes of the studied variables on socioeconomic systems, the population of coastal municipalities from the 1982, 1992, 2002, 2012, and 2017 censuses (INE 2017) is analyzed. Data are lumped and analyzed at 19 points every 2° of latitude.

# 4 Results

## 4.1 Decadal trends for individual variables

### 4.1.1 Atmospheric pressure, alongshore wind, and *SST*

Except for the southernmost point (55°S), an increase in *Pa* is observed throughout the country (Fig. 2a), with major growths between 36°S and 48°S. The alongshore wind variability on the CCZ is driven primarily by surface pressure gradients; the cross-shore pressure gradient produces geostrophic alongshore winds and the alongshore pressure gradient also forces an alongshore semi-geostrophic flow due to the presence of coastal mountains (Muñoz and Garreaud 2005; Rahn and Garreaud 2014). Then, the latitudinally different trends of *Pa* result in trends of the alongshore pressure gradient which are expected to trigger variations in coastal
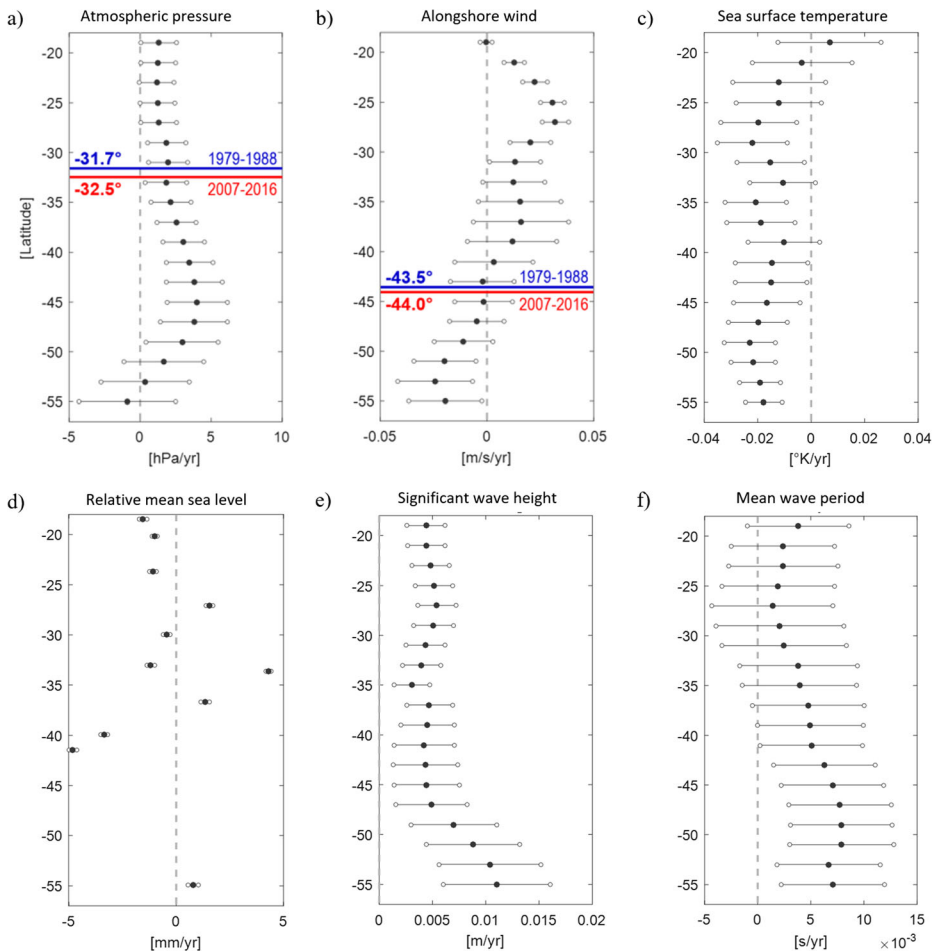
**Fig. 2** **a–l** Slope of linear trends for all variables within the CCZ. Dots represent the estimated slope while 95% confidence intervals are shown in horizontal bars and circles. **l** Coastal cities with tide gauges throughout the CCZ. The position of the SPSA (**a**) and the location where westerly winds bifurcate equatorward and poleward (**b**) is depicted for 1979–1988 and 2007–2016

upwelling. In fact, Aguirre et al. (2018) showed that both the cross-shore and alongshore pressure gradients have experimented a positive trend during the last decades, particularly between 35°S and 45°S, along with the poleward migration of ~0.8° in the SPSA (from 31.7°S to 32.5°S), consistent with earlier findings (Schneider et al. 2017; Aguirre et al. 2018).

Alongshore winds show an increasing trend over the upwelling region (18°S–40°S), and a change of sign southward (Fig. 2b). Since the positive (negative) values of *Ua* represent northward (southward) flow, the negative trends of alongshore winds south 45°S mean positive trends in magnitude. Then, results show an increase of up to 0.03 m s year$^{-1}$ in wind speed over the whole region. The location where westerly winds bifurcate in equatorward and poleward winds also shows a poleward migration of ~0.5° (from 43.5°S to 44.0°S) between the two periods. In addition, *SST* trends show that a water cooling of ~0.02°K year$^{-1}$ has occurred south of 21°S (Fig. 2c), consistent with previous findings in the Southeast Pacific (Falvey and Garreaud 2009; Ancapichún and Garcés-Vargas 2015; Schneider et al. 2017).
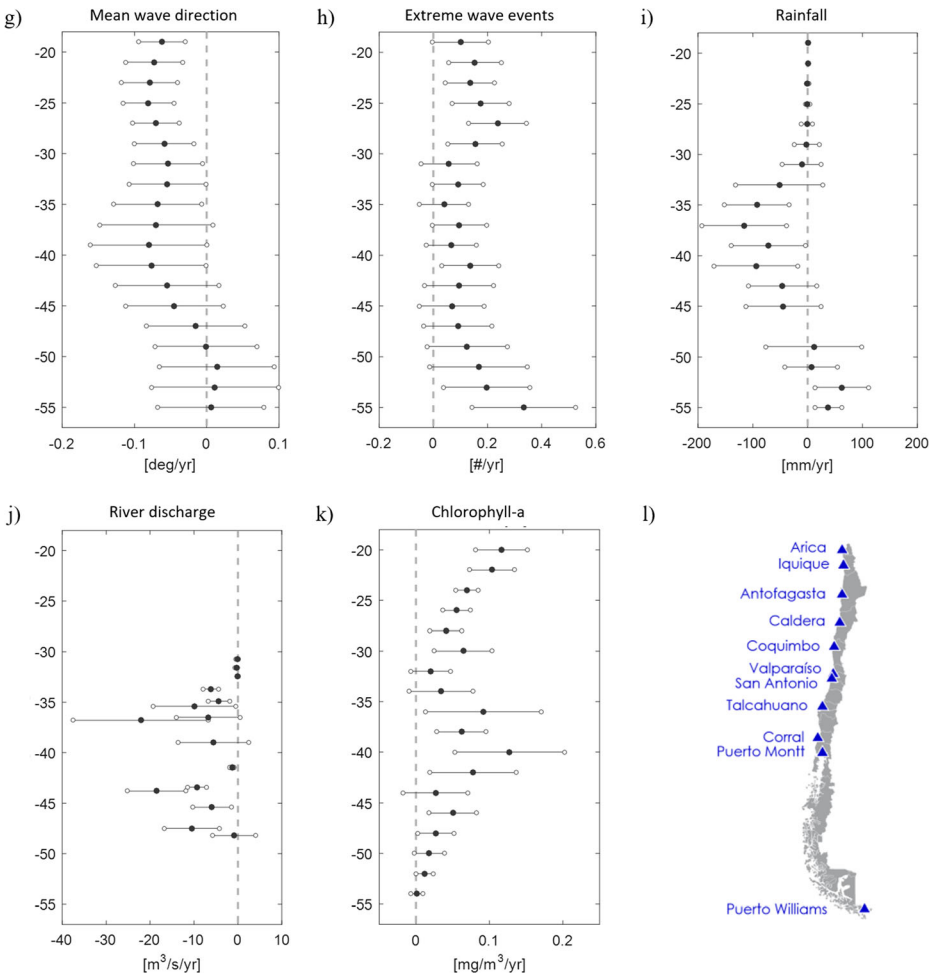
Fig. 2 (Continued)

### 4.1.2 Rainfall, river discharge, and chlorophyll-a

With exceptions in the north (18°S–25°S) and south (> 50°S), rainfall shows negative trends (Fig. 2i, Figure A10, supplementary material), with rates fluctuating between − 0.09 and − 116.06 mm year^{-1}. These trends are partly explained by meteorological droughts, occurring when dry weather patterns dominate the South American region (Seth et al. 2013). Since 2010, central Chile experienced a long period of droughts which has been attributed 25% to anthropogenic climate change (Boisier et al. 2016). The persistent water deficit, enhanced by this drought, has resulted in major reductions of surface runoff with significant ecological and socioeconomic repercussions (Garreaud et al. 2017).

Except for few cases, there is a clear reduction in river discharge (Fig. 2j), with trends between − 0.17 and − 22.13 m³ s⁻¹ year⁻¹, and more marked deficits within the central Chilean watershed (i.e., Biobio river). These differences reflect the north-to-south precipitation gradient, as well as the differences in catchment areas.

| | 19°S | 21°S | 23°S | 25°S | 27°S | 29°S | 31°S | 33°S | 35°S | 37°S | 39°S | 41°S | 43°S | 45°S | 47°S | 49°S | 51°S | 53°S | 55°S | Correlations \|R²\|≥0.5 |
|---|---|---|---|---|---|---|---|---|---|---|---|---|---|---|---|---|---|---|---|---|
| Hs - Dm | 0.0 | 0.0 | -0.1 | -0.1 | -0.2 | -0.4 | -0.3 | -0.2 | -0.1 | -0.1 | | 0.1 | 0.1 | 0.1 | 0.2 | 0.2 | 0.2 | 0.2 | 0.2 | |
| Hs - Tm | 0.6 | 0.5 | 0.4 | 0.4 | 0.2 | 0.1 | 0.1 | 0.2 | 0.2 | 0.4 | 0.4 | 0.5 | 0.4 | 0.5 | 0.5 | 0.6 | 0.7 | 0.7 | 0.7 | 7 |
| Hs - Pa | 0.2 | 0.2 | 0.2 | 0.2 | 0.1 | 0.2 | 0.2 | 0.2 | 0.2 | 0.1 | 0.0 | -0.1 | -0.2 | -0.3 | -0.3 | -0.4 | -0.5 | -0.5 | -0.5 | 2 |
| Hs - SST | | 0.1 | -0.1 | -0.1 | -0.2 | -0.2 | -0.2 | -0.1 | -0.1 | 0.0 | 0.0 | 0.1 | | -0.1 | -0.1 | -0.1 | -0.2 | -0.2 | -0.2 | |
| Hs - Ua | 0.2 | 0.3 | 0.3 | 0.3 | 0.4 | 0.5 | 0.5 | 0.4 | 0.2 | 0.1 | -0.1 | -0.2 | -0.4 | -0.3 | -0.4 | -0.5 | -0.6 | -0.8 | -0.8 | 5 |
| Dm - Tm | 0.3 | 0.3 | 0.3 | 0.3 | 0.3 | 0.5 | 0.4 | 0.3 | 0.1 | 0.1 | -0.1 | -0.2 | -0.2 | -0.2 | -0.1 | | 0.2 | 0.3 | 0.4 | 1 |
| Dm - Pa | | | 0.0 | 0.0 | -0.1 | -0.3 | -0.4 | -0.6 | -0.6 | -0.6 | -0.6 | -0.6 | -0.6 | -0.5 | -0.5 | -0.5 | -0.4 | -0.4 | | 7 |
| Dm - SST | 0.1 | 0.1 | 0.1 | 0.2 | 0.2 | 0.2 | 0.2 | 0.3 | 0.3 | 0.3 | 0.2 | 0.2 | 0.1 | 0.1 | 0.1 | 0.1 | 0.1 | 0.2 | 0.2 | |
| Dm - Ua | -0.1 | -0.2 | -0.3 | -0.3 | -0.4 | -0.6 | -0.7 | -0.7 | -0.7 | -0.8 | -0.8 | -0.8 | -0.8 | -0.8 | -0.8 | -0.8 | -0.8 | -0.6 | -0.6 | 14 |
| Tm - Pa | 0.2 | 0.2 | 0.2 | 0.2 | 0.2 | 0.1 | 0.1 | 0.1 | 0.1 | 0.2 | 0.3 | 0.4 | 0.3 | 0.3 | 0.2 | 0.1 | -0.1 | -0.3 | -0.3 | |
| Tm - SST | -0.1 | 0.0 | 0.0 | 0.0 | | | | | 0.1 | 0.1 | 0.1 | 0.1 | 0.1 | 0.1 | 0.1 | 0.1 | | -0.1 | 0.0 | |
| Tm - Ua | -0.3 | -0.4 | -0.5 | -0.5 | -0.5 | -0.5 | -0.4 | -0.2 | -0.2 | -0.1 | | 0.1 | | -0.1 | -0.2 | -0.3 | -0.5 | -0.7 | -0.7 | 4 |
| Pa - SST | -0.6 | -0.5 | -0.5 | -0.5 | -0.4 | -0.3 | -0.3 | -0.3 | -0.3 | -0.3 | -0.2 | -0.1 | 0.0 | | 0.1 | 0.1 | 0.1 | 0.1 | 0.1 | 3 |
| Pa - Ua | -0.1 | 0.0 | | 0.1 | | 0.3 | 0.4 | 0.5 | 0.6 | 0.7 | 0.7 | 0.7 | 0.6 | 0.6 | 0.5 | 0.5 | 0.4 | 0.5 | 0.4 | 8 |
| SST - Ua | 0.2 | 0.1 | 0.1 | 0.0 | -0.1 | -0.2 | -0.2 | -0.2 | -0.3 | -0.3 | -0.2 | -0.1 | -0.1 | | 0.1 | 0.1 | 0.1 | 0.1 | 0.1 | |
| correlations \|R²\|≥0.5 | 2 | 2 | 1 | | 1 | 3 | 1 | 2 | 3 | 3 | 3 | 3 | 3 | 3 | 4 | 3 | 4 | 5 | 5 | |

**Fig. 3** Latitudinal distribution of correlations between variables. Values in red (blue) represent positive (negative) values of the coefficient of determination $R^2$. Variables correspond to the significant wave height (*Hs*), mean wave direction (*Dm*), mean wave period (*Tm*), Pa, alongshore winds (*Ua*), and sea surface temperature (*SST*). Cells in white have $|R^2| < 0.1$. The last row and column show the number of significant correlations arbitrarily defined herein by $|R^2| \geq 0.5$. Cells in white correspond to 0. Negative correlations between *Ua* and *Hs* are explained by the fact that poleward (negative) alongshore winds increase results in higher waves in high latitudes

Finally, a positive trend in chlorophyll-a, with values ranging between 0.001 and 0.13 mg m$^{-3}$ year$^{-1}$, is observed (Fig. 2k). These trends agree with previous studies reporting increased chlorophyll-a along EBUS (Gregg et al. 2005; Marrari et al. 2017) which may be attributable to an increase and along coast wind.

### 4.1.3 *RMSL*

*RMSL* trends (Fig. 2d) show a heterogeneous distribution, with some stations revealing an increase of up to 4.30 mm year$^{-1}$ (San Antonio) or reductions of up to $-4.83$ mm year$^{-1}$ (Puerto Montt). Except for Caldera, northern stations covering an area of nearly 1600 km show rates of $-1.56$ to $-0.45$ mm year$^{-1}$, probably associated to coastal uplift driven by plate coupling built up since the 1877 megathrust earthquake (Métois et al. 2013). The central region shows an alternation of rising and falling trends, with maximum values in San Antonio and lower values in Talcahuano. Considerable differences between the neighboring stations could be attributable to differences in seismicity (e.g., Comte et al. 1986) or local effects (i.e., while the tidal gauge in Valparaíso is located in a rocky formation, in San Antonio, the instrument is sited near a river outlet). Toward the south, Corral and Puerto Montt show the largest drops throughout the country, which may still be affected by the subsidence triggered by the 1960 Valdivia Earthquake (Plafker and Savage 1970). In Puerto Williams, the *RMSL*

seems to be less affected by seismicity, since the relative motions of tectonic plates occur at relatively lower speeds (Perucca et al. 2016). South stations may also be affected by glaciation-induced sea-level change during the Holocene (Milne et al. 2005; Reyes et al. 2018), though these changes are significantly smaller than coseismic uplift/subsidence.

### 4.1.4 Wave climate

Significant wave heights show an increase of 0.003~0.011 m year$^{-1}$ between 1980 and 2015, being spatially stable north of 47°S and considerably larger southward (Fig. 2e). This range is equivalent to an increase of 0.1~0.4 m for the analyzed period, which is considerable (10–20%) compared with the annual mean of 2 to 4 m throughout the country (Beyá et al. 2016, Fig. 1a). These results are consistent with those found by Young et al. (2011), who estimate an increase of 5 to 10% in *Hs* based on 23 years (1985–2008) of satellite altimeter measurements in the South Pacific.

Mean wave periods show an increase of 0.001~0.008 s year$^{-1}$, with minor changes to the north and maximum increments toward the south of the country (Fig. 2f). This shift implies an increase below 0.3 s between 1980 and 2015, which is rather small (0.4~3.5%) compared with the absolute values of 8 to 10 s throughout the country (Beyá et al. 2016). Regardless of the positive trends between 19°S and 37°S, confidence intervals reach negative values, making any conclusion arguable in this region.

Figure 2g depicts a southward rotation of the mean wave direction of ~ 0.1° year$^{-1}$ between 19°S and 41°S, which is equivalent to 3.5° between 1980 and 2015. Amid 43°S and 49°S, the trend is still negative, but the confidence interval covers both positive and negative values. Between 51°S and 55°S, there is a slight northward rotation in *Dm*, but these results are questionable considering the large confidence intervals.

A generalized increase in the annual rate of extreme wave events is observed throughout the country, with positive rates between 0.1 and 0.3 events year$^{-1}$ (Fig. 2h, Figure A9, supplementary material). This is equivalent to 4 to 12 more events annually in 2015 compared with the early 1980s. Martínez et al. (2018) observed an increment of 0.32 events year$^{-1}$ between 1958 and 2016 in Valparaíso, whereas the present study indicates a lower increase of 0.11 events year$^{-1}$ in the same site between 1980 and 2015. Martinez et al.'s study, however, patches two datasets, one of which is validated in central Chile (Beyá et al. 2017) while the other is not. Additionally, both studies cover different periods of time, making any comparison biased. The increasing number of extreme wave events will have important consequences in port operability and coastal flooding along the CCZ (Camus et al. 2017).

### 4.2 Demographics

The 2017 census (INE 2018) indicates that among the 17.6 million inhabitants, 4.5 million lived in one of the 100 coastal municipalities and nearly 1 million in Low Elevation Coastal Zones (LECZ) below 10 m above sea level (MMA 2019). The limited area of LECZ within the country (15.752 km², MMA 2019) is relatively small due to the presence of high coastal terraces resulting from plate tectonics. The 5% of inhabitants in LECZ is lower than the global and Latin American averages of 10% and 6%, respectively (McGranahan et al. 2007). The northern desert is sparsely inhabited, with the exceptions of coastal cities which economy is mainly associated to mining (Fig. 1b). The most populated coastal regions include the metropolitan areas of Valparaíso and Concepción (37°S), each having nearly 1 million

inhabitants; these cities belong to a region strongly affected by coastal upwelling which concentrates numerous fishing coves and industrial fishing. Patagonia has significantly smaller population due to the complex geomorphology, limited connectivity, and harsh climate. The region is characterized by a strong expansion of aquaculture farming. Among the 106.544 km of coastline (MMA 2019), 2% are urban and 98% rural (CIESIN 2013).

### 4.3 Correlations among anomalies of variables

Due to the considerable length and the north-south orientation of the CCZ traversing different climate types, correlations show smooth latitudinal gradients which may even change signs latitudinally (Fig. 3). Overall, there are few pairs of variables that sharply correlate ($|R^2| \geq 0.5$) with a linear regression model, while others not ($|R^2| < 0.5$).

There is a positive correlation between $Hs$ and $Tm$ in extreme north (19°S–21°S) and south (45°S–55°S) of the CCZ. Previously, $Hs$ has been related with the SAM index in the South Pacific, particularly during austral winter (Hemer et al. 2010). The positive (negative) phase of the SAM is associated with a strengthening (weakening) and poleward (equatorward) shift of the storm-track over the Southern Ocean (Thompson et al. 2000; Fyfe 2003). Then, a positive correlation between $Hs$ and $Tm$ along the Southeast Pacific is foreseeable, because an intensification of winds in the Southern Ocean generates higher waves, and waves generated further south have larger periods due to its propagation on larger distances to the CCZ. The lower values of correlations found in central Chile (27°S–35°S) could be related to the presence of an atmospheric coastal low-level jet (Garreaud and Muñoz 2005) that introduce energy to lower periods in the spectrum, thus increasing $Hs$ and decreasing $Tm$.

There is a negative correlation between $Hs$ and $Pa$ in extreme south (53°S–55°S), where locally generated waves provide an important contribution to the total wave energy (Semedo 2011; Fan et al. 2014). Thus, lower local atmospheric pressure could be related to more frequent and/or more intense extratropical cyclones, strengthening surface winds and increasing wave heights.

A strong relationship between alongshore winds and wave parameters at high latitudes where waves are generated (49°S–55°S) is found ($Ua$-$Hs$ and $Ua$-$Tm$). There is no correlation between $Ua$ and $Hs$ elsewhere, consistent with the fact that $Hs$ is mainly controlled by swells generated throughout the Pacific Ocean. Nevertheless, in central Chile (27°S–33°S) positive correlations between $Hs$ and $Ua$ could be explained by the presence of an atmospheric coastal low-level jet that is able to introduce an important amount of energy to the spectra, thus increasing $Hs$ during spring and summer (Aguirre et al. 2017).

There is a strong positive correlation between $Pa$ and $Ua$ in central and south of Chile (33°S–47°S), showing that increased (decreased) $Pa$ in this region results in more (less) intense coastal pressure gradients triggering alongshore winds (Rahn and Garreaud 2014) and therefore coastal upwelling processes. On the other hand, strong negative correlations between $Ua$ and $Dm$ are found south of 29°S. As $Ua$ is the alongshore wind, it introduces local generated waves coming from south (north) when it blows equatorward (poleward), thus impacting $Dm$. In addition, negative correlations found between $Dm$ and $Pa$ in mid to south latitudes (35°S–47°S) could be explained by transitivity, as $Ua$ and $Pa$ are strongly correlated.

There are moderate negative correlations between $Pa$ and $SST$ in northern Chile. This could be explained as the coastal cooling seems to be part of a larger scale La Niña–like pattern (Garreaud and Falvey 2009). Then, an intensification of the SPSA results in increased local $Pa$ which is likely to play a major role in decrease temperatures off the coast of northern Chile.

The physical explanation of the apparent negative *Pa-SST* relationship is likely to reside in the enhancement of upwelling-favorable winds along the coast, which in turn produce offshore transport and coastal cooling. In fact, a significant relationship between *Ua* and *SST* has been showed in the synoptic scale (Renault et al. 2009; Aiken et al. 2011).

There are no significant correlations between *Hs* and *Tm* with *Dm* throughout the country. Though high correlations could be expected in relatively small water bodies, the existence of different source regions of waves throughout the Pacific Ocean tends to decouple the mean wave direction from heights and periods. This becomes evident in the offshore directional wave spectra obtained at different latitudes (Figure A12, supplementary material).

# 5 Discussion

## 5.1 Climate variability in the CCZ

Due to the short period of analysis, long-term trends computed herein may be overshadowed or amplified by climate variability. The SAM, for example, is the major mode of variability in the atmospheric circulation of the mid to high latitudes in the southern hemisphere. Observations and simulations have shown a trend toward the positive phase of the SAM during the last decades (Marshall 2003; Gillett and Fyfe 2013) which has been attributed to the anthropogenic influence from a combination of increasing greenhouse gases and ozone depletion (Gillett et al. 2013). In other terms, although the PDO is a measure of a *SST* mode of variability in the North Pacific (Zhang et al. 1997; Mantua et al. 1997), evidence highlights that the Pacific decadal variability exhibits a pattern of symmetric atmospheric circulation changes of the Northern and Southern Hemispheres (Garreaud and Battisti 1999). The dominant spatial signatures of *SST*, *Pa*, and wind stress associated with this decadal variability may be described as ENSO like due to the similar spatial patterns of interannual anomalies associated with ENSO (Zhang et al. 1997). The PDO index has evolved in a negative trend during the last three decades; after an abrupt shift in the 1970s from a negative to a positive phase, it shifted to negative values in the late 1990s, after the 1997/1998 El Nino event (Newman et al. 2016). Observed *Pa* and precipitation trends in Chile are consistent with the expected—La Niña–like—response to the PDO (Boisier et al. 2016). Furthermore, the intensity and position of the SPSA, the coastal *SST*, and thermocline depth have been also related to the Pacific decadal variability at the Southeast Pacific (Montecinos et al. 2003; Pizarro and Montecinos 2004; Ancapichún and Garcés-Vargas 2015). Despite these early findings, additional modelling efforts and a strengthening of data acquisition techniques are required to further discriminate the contribution of climate variability and climate change on these observed trends.

## 5.1.1 Atmospheric pressure, alongshore wind, and *SST*

We show that *Pa* has increased particularly at south-central Chile. This spatial pattern is consistent with a strengthening, expansion, and southward migration of the SPSA observed in recent decades (e.g., Aguirre et al. 2018; Flores-Aqueveque et al. 2020). Indeed, the SPSA strengthened by 2 hPa between 2002 and 2013 (Schneider et al. 2017) and its southward migration was detected around 35°S–36°S over the south eastern Pacific Ocean (Ancapichún and Garcés-Vargas 2015; Aguirre et al. 2018), probably due to the poleward expansion of the Hadley cell (Hu and Fu 2007). These changes have led to an intensification of the upwelling-

favorable winds in northern Chile and an expansion of the upwelling regime southward (Fig. 2b). The increased Ekman suction and its offshore transport would explain much of the observed coastal cooling shown in Fig. 2c (Falvey and Garreaud 2009; Schneider et al. 2017).

Several climate models indicate that recent changes in the SPSA and upwelling-favorable winds will continue during the next decades as consequence of global warming (Bindoff et al. 2019). Under different climate change scenarios, a strengthened and expanded SPSA along with its poleward displacement is expected (e.g., Belmadani et al. 2014). In fact, the spatial patterns of recent decadal trends in *Pa*, *Ua*, and *SST* off Chile are consistent with those projected in warming scenarios. Particularly, the EBUS off south-central Chile is expected to exhibit forthcoming changes in timing, intensity, and spatial distribution of alongshore winds (Wang et al. 2015; Aguirre et al. 2019).

Over past decades (1979–2016), the PDO index has shown a negative trend impacting *Pa* trends at high and mid-latitudes of the South Pacific (Boisier et al. 2016), *SST* trends along the coast of Chile (Falvey and Garreaud 2009), and the intensity and position of the SPSA, with consequences in upwelling-favorable winds trends in the Humboldt System (Ancapichún and Garcés-Vargas 2015, Aguirre et al. 2018). However, climate attribution has shown that the PDO index can only partly explain the negative *SST* trends at the Southeast Pacific in recent decades (Falvey and Garreaud 2009) and that changes in *Pa* can be largely attributable to the PDO in the central-south Pacific. Thus, PDO represents only a slight contribution to observed *Pa* trends at the CCZ.

The observed poleward drift of the upwelling regime (40°S–55°S) in the whole country could be attributable to the positive trend in the SAM index (Thompson et al. 2000) explained by loss of photochemical ozone in the stratosphere (Thompson and Solomon 2002) and/or anthropogenic increment of greenhouse gases in the atmosphere (Fyfe et al. 1999). The positive phase of the SAM is associated with negative *Pa* anomalies in high latitudes (~65°S), positive *Pa* anomalies in mid-latitudes (~40°S), a strengthened and poleward shifted circumpolar westerly wind, anomalously dry conditions over southern South America due to the southward shift of the storm tracks, among others. The SAM could partially explain the spatial pattern of the positive trends of *Pa* in southern Chile, which decrease at higher latitudes to become negative at 55°S. Furthermore, local surface forcing by the SAM explains *SST* anomalies (e.g., Screen et al. 2009) showing a strong annular pattern with cooling (warming) southward (northward) of ~45°S during the positive phase of the SAM index (Gupta and England 2006).

### 5.1.2 Rainfall, river discharge, and chlorophyll-a

Climatologically, there is a latitudinal increase in rainfall from around 100 mm year$^{-1}$ in the extreme north to 2000 mm year$^{-1}$ in the south of the country (Aravena and Luckman 2009), the majority of which originates in winter from cold fronts associated with migratory low-pressure systems embedded in the mid-latitude westerlies (Fig. 1a, Fuenzalida 1982). Additionally, cutoff lows contribute to ~5 to 10% of the annual rainfall between 26°S and 36°S (Pizarro and Montecinos 2000). The relatively large number of fronts passing through central Chile during winter is due to the seasonal changes in large-scale circulation, specifically the movement of the subtropical SPSA and the subtropical jet stream, which are situated at their northernmost position during this time. Regarding climate variability, the displacement and intensification of the SPSA in central and southern Chile (30°S–45°S) affects the rainfall regime, thus the flow of freshwater to coastal systems (Garreaud et al. 2017).

The generalized reduction in river discharge observed in the analyzed period could be caused by natural drivers and/or water deficits caused by a larger human demand. It is widely acknowledged that rainfall deficit is associated, although not necessarily in phase, with a water supply deficit (i.e., soil moisture, streamflow, groundwater, and reservoir levels). Additionally, drought-related water shortages could be a consequence of the climatic variability of water catchments due to a combination of natural variability and anthropogenic climate change.

The sequence of dry years since 2010 corresponding to the longest event on record (Garreaud et al. 2019) could also play a role. As previously discussed, that the negative trend of the PDO, the positive trend of the SAM and the anthropogenic forcing (increase of greenhouse gases concentration and stratospheric ozone depletion) contribute to the strength and longevity of this drought (e.g., Boisier et al. 2016, Garreaud et al. 2019, Boisier et al. 2019). This phenomenon has reduced the river discharge, producing several ecological consequences in the marine ecosystem. The plume areas diminished by about 50% compared with historical values, significantly reducing the size of the chlorophyll-a pool within plumes off the coast during southern hemisphere's late winter and early spring (Masotti et al. 2018). Another consequence is the reduction in freshwater discharge from Itata to Biobio Rivers, which triggered a decrease between 25 and 75% of nitrate and phosphate export to the coastal zone between May and September (Masotti et al. 2018). The significant dependency of nutrients availability in coastal waters from river discharge between 2000 and 2017 is illustrated Figure A11 (supplementary material). These nutrients are essential for phytoplankton growth, and, as a result, the spawning (mainly in winter), larval development, and feeding of pelagic fish such as anchovies and sardines, which have a great economic importance for the country (Quiñones and Montes 2001). Finally, changes in the quantity of freshwater discharge also affect the buoyancy and stratification of the water column, which alters heat and gas exchange between coastal waters and the atmosphere (Mann and Lazier 2006). The real role of natural and anthropogenic drivers on the reduction of river discharge should be subject of future research.

Finally, in the East South Pacific region, positive trends in chlorophyll-a could be explained by the increased upwelling-favorable winds (Aguirre et al. 2018), that pump nutrients toward the surface to promote an increase in phytoplankton biomass, which may have repercussions on the oxygen consumption, nitrification, and organic matter mineralization in the aphotic layer, leading to nitrous oxide accumulation (Farías et al. 2015).

### 5.1.3 *RMSL*

Changes in *RMSL* are caused by a combination of climate-driven changes in both the ocean surface and the seafloor. This variable results from a combination of long-term climate drivers, variability, short-term meteorological phenomena (storm surge, meteotsunamis, and infragravity waves), astronomical tides, and vertical changes in the earth's crust acting at different spatial-temporal scales. Secular subsidence (i.e., slow process occurring after a load is applied) due to natural and anthropogenic causes, as well as changes caused in the seismic cycle (Wesson et al. 2015), also plays an important role in subduction zones.

Being one of the most seismically active margins on the planet (Giesecke et al. 2004), *RMSL* changes due to climate drivers seem to be minor when compared with crustal deformations triggered by subduction earthquakes. Indeed, vertical displacements of various meters triggered during the 1960 Valdivia (Plafker and Savage 1970), 1985 Valparaíso (Castilla 1988) and 2010 Maule (Farías et al. 2010) earthquakes are comparable with centuries of sea level rise due to climate change. Indeed, the absolute mean sea level (*AMSL*) is expected to rise between

0.34 and 0.74 m over the CCZ by the end of twenty-first century (Albrecht and Shaffer 2016). In addition, Montecino et al. (2017) indicate that the crustal deformation during the interseismic period is faster than that of *AMSL*. ENSO events are also responsible for significant changes in *AMSL*, causing a rise (drop) of up to 30~40 cm during strong El Niño (La Niña) years (Enfield and Allen 1980; Reguero et al. 2015). Finally, to our level of knowledge, there are no studies connecting the PDO or SAM to *RMSL* in the CCZ.

The distinctive features of the CCZ, where sea level rise driven by climate change may be overshadowed by coseismic deformation and climate variability, can be used to understand the long-term effects in coastal environments due to climate change. For example, the subsidence of nearly 2 m caused by the 1960 Valdivia earthquake (Plafker and Savage 1970) is comparable to nearly 600 years of climate-driven *AMSL* rise, according to global trends of 3.2 mm year$^{-1}$ estimated for 1993–2010 (Church et al. 2013). This earthquake dramatically transformed low-lying areas used for agriculture into wetlands (Saint-Amand 1963), in a way that can be envisaged in exposed areas as the century evolves. Finally, coseismic seafloor changes due to megathrust earthquakes can either have positive or negative impacts; while coseismic subsidence in combination with sea level rise may have catastrophic consequences in lowlands, coastal uplift may reduce the impacts of long-term changes in sea level.

### 5.1.4 Wave climate

Several studies reveal that both mean (Hemer et al. 2010) and extreme wave climate (Izaguirre et al. 2011) in the Southern Ocean are largely controlled by variability in the SAM. Furthermore, some studies describe remarkable changes in the high-latitude Southern Hemisphere synoptic environment over recent decades, such as the change in the number of cyclones (Simmonds and Keay 2000). Research based on cyclone-tracking techniques show that the number of cyclones between 40°S and 60°S has decreased, while there has been a poleward increase in cyclone number during the last 30 years at latitudes greater than 60°S (Fyfe 2003). Changes in atmospheric surface circulation are largely consistent with trends in wave climate obtained herein, namely the increase in *Hs* and *Tm*, as well as a southward rotation in *Dm* between 19° and 47°S, which could have consequences on the geometry of relatively long and exposed sandy beaches, though local studies (Martínez et al. 2018) are still conclusive. These changes could be attributed to both the positive trend of the SAM during the last few decades (Thompson et al. 2000).

### 5.2 Impacts on coastal population

According to Church et al. (2013), the rapid increase in coastal population will boost the risk of climate-related disasters. The CCZ is highly vulnerable to climate change since it is prone to natural hazards including droughts, sea level rise, coastal storms, strong winds, and rainfall (Aguirre et al. 2018, Garreaud et al. 2019), whose consequences are important given the increasing frequency and intensity at which they occur (IPCC 2019) as well as the growth in local population (Fig. 1b). Indeed, MMA (2019) estimates that nearly 47,000 people currently live in 19,000 households that will be flooded in Chile by a combination of sea level rise and coastal storms by 2045. These areas are inhabited by ocean-dependent workers, whether offering services or working as fishermen and fish farmers. Nearly 500 coastal settlements on the CCZ have a great dependence on ocean resources, while 171 port facilities, 546 small fishing harbors, and 475 different types of coastal works will be subjected to more intense conditions in the next decades (MMA 2019). Additionally, they project a generalized beach

erosion, reduction of coastal wetlands, an increase in infrastructure damage and negative impacts in the operation of industrial and fishing ports because of sea level rise and an increase in the frequency and intensity of coastal storms. However, the impacts of sea level rise in Chile are minor compared with those in other developing countries (Dasgupta et al. 2007) due to the presence of high coastal terraces throughout the CCZ. Along with these climate-driven effects, anthropogenic impacts include marine pollution of metals due to mining in the north, agrochemical and organic matter due to agriculture in central Chile, and aquaculture in Patagonia, among others. Coastal risk reduction needs to be based on a comprehensive approach considering anthropogenic, geophysical, biogeochemical, and climate-driven perturbations.

This region also includes the most biological productive EBUS, which, as analyzed, is subject to an intensification shown in chlorophyll-a trends (Fig. 2k). These changes, whose mechanisms and future projections are still uncertain, collide with increases in wind, stratification/turbulence, offshore water exportation, and therefore with nutrient levels, levels of acidification, oxygen, and microalgal biomass, including even harmful algal bloom with concomitant consequences in marine fisheries (Aguirre et al. 2018; Iriarte 2018; León-Muñoz et al. 2018; Soto et al. 2019). Management of fisheries and other marine resources in EBUS should thus be improved by better understanding how nutrient enrichment and primary production are related to upwelling processes, and how they are likely to change in the future (Bindoff et al. 2019).

Current adaptation efforts, such as the climate change framework law currently in parliament (MMA 2020), or adaptation plans which are approved (biodiversity, cities, infrastructure), under review (fisheries and aquaculture) or discussion (coastal zone, tourism), should be strongly enforced to cope with climate-driven environmental and socioeconomic impacts which are already ubiquitous.

### 5.3 Improvement of coastal long-term monitoring systems

Chile's CCZ is economically, culturally, and socially dependent on the ocean and its resources. Yet, there is a lack of long-term and real-time observations to respond to climate change and fast perturbations in the ocean and atmosphere. However, there is an immense disparity between the availability of data on land and in the ocean. As example, for inland climatology, there are nearly 2300 instruments (CR$^2$ 2019) while the seismological network is composed of 492 devices (Barrientos 2018). In the ocean, however, SHOA operates only 45 tide gauges (shoa.cl/php/nivel-del-mar.php?idioma=es) and has intermittently deployed offshore wave buoys which records are relatively short. Efforts should be carried on a nationwide level to develop oceanographic networks and open databases following examples elsewhere (e.g., Hamilton 1980; Clemente 2001).

Recently, the Chilean scientific community proposed an Integrated Observing System for the Southeast Pacific Ocean (SIOOC), consisting of an array of instruments for monitoring and forecasting several variables (CC-COP25 2019). Its implementation would require the integration of existing observational systems, acquisition of state-of-the-art equipment (oceanic, atmospheric, computational, real-time transmission, and database management systems), development of data management protocols, periodic maintenance, calibration facilities, and highly qualified technicians to implement and maintain the system. Such a network could be applied in climate change monitoring, early warning systems for coastal hazards (e.g., storm surges, tsunamis, harmful algal blooms, hypoxia, eutrophication, contaminants), operational systems for weather, port and aquaculture, monitoring of marine protected areas, and regional/global models of atmospheric, ocean, and biogeochemical variables. The system could also aid

in the elaboration of public policies based on environmental evidence, and in the provision of critical information for scientists, policymakers, stakeholders, and citizens. Priority on which variables to choose and where to measure should be established after a comprehensive study; however, the lack of an offshore wave gauge network is evident since available hindcast (e.g. Beyá et al. 2017) is locally validated from satellite tracks and a limited amount of wave buoys.

## 6 Conclusions

A long-term analysis of atmospheric, hydrologic, oceanographic, and biogeochemical variables is conducted to identify linear trends of variables and interannual correlations among anomalies of the herein described variables in the CCZ. The analysis shows that the strengthening, expansion, and southward migration of the SPSA may partially explain the increase in atmospheric pressure and alongshore (equatorward) winds and the reduction in SST, while the reduction in rainfall and river discharge has multiple causes which relative importance is yet unknown. Historical *RMSL* trends are spatially heterogeneous and probably shaped by the vertical deformation of the seafloor within the seismic cycle, which is comparable with centuries of climate-driven sea level changes. Extreme sea level projections should therefore be complemented with local estimates of subsidence/uplift due to sediment compaction, isostatic rebound, and earthquakes. Significant wave heights have increased moderately, periods have marginally changed, and a southward rotation in the offshore wave direction is observed, while the number of extreme wave events increased between 4 and 12 events since the early 1980s in the northern and southernmost ends of the country. Though some clear trends and correlations in datasets of 35 years are evidenced, the influence of climate variability (PDO, SAM) may affect the trends due to the short data length. Thus, a strengthening of data acquisition systems and additional attribution efforts should be conducted to isolate the influence of climate variability, climate change anthropogenic, and geophysical forcings on these trends.

**Author contribution** CA analyzed atmospheric variables, PW-MC wave climate and correlations, and LF-IM river discharge and chlorophyll-a. PW-LF-CA drafted the manuscript with major revisions by coauthors.

## References

Aguirre C, Rutllant JA, Falvey M (2017) Wind waves climatology of the Southeast Pacific Ocean. Int J Climatol 37(12):4288–4301

Aguirre C, García-Loyola S, Testa G, Silva D, Farias L (2018) Insight into anthropogenic forcing on coastal upwelling off south-central Chile. Elem Sci Anth 6(1)

Aguirre C, Rojas M, Garreaud RD, Rahn DA (2019) Role of synoptic activity on projected changes in upwelling-favourable winds at the ocean's eastern boundaries. npj. Clim Atmos Sci 2(1):1–7

Aiken CM, Navarrete SA, Pelegrí JL (2011) Potential changes in larval dispersal and alongshore connectivity on the central Chilean coast due to an altered wind climate. J Geophys Res Biogeosci 116(G4)

Albrecht F, Shaffer G (2016) Regional sea-level change along the Chilean Coast in the 21st century. J Coast Res 32(6):1322–1332

Ancapichún S, Garcés-Vargas J (2015) Variability of the Southeast Pacific subtropical anticyclone and its impact on sea surface temperature off north-central Chile. Ciencias Marinas 41(1):1–20

Aravena JC, Luckman BH (2009) Spatio-temporal rainfall patterns in southern South America. Int J Climatol 29(14):2106–2120

Barrientos S (2018) The seismic network of Chile. Seismol Res Lett 89(2A):467–474

Belmadani A, Echevin V, Codron F, Takahashi K, Junquas C (2014) What dynamics drive future wind scenarios for coastal upwelling off Peru and Chile? Clim Dyn 43(7–8):1893–1914

Beyá J, Álvarez M, Gallardo A, Hidalgo H, Aguirre C, Valdivia J, Parra C, Méndez L, Contreras C, Winckler P, Molina M (2016) Atlas de Oleaje de Chile. ISBN: 978-956-368-194-9. https://oleaje.uv.cl/

Beyá J, Álvarez M, Gallardo A et al (2017) Generation and validation of the Chilean Wave Atlas database. Ocean Model 116:16–32

Bindoff NL, Cheung WWL, Kairo JG, Arístegui J, Guinder VA, Hallberg R, Hilmi N, Jiao N, Karim MS, Levin L, O'Donoghue S, Purca Cuicapusa SR, Rinkevich B, Suga T, Tagliabue A, Williamson P (2019) Changing ocean, marine ecosystems, and dependent communities. In: IPCC special report on the ocean and cryosphere in a changing climate

Boisier JP, Rondanelli R, Garreaud RD, Muñoz F (2016) Anthropogenic and natural contributions to the Southeast Pacific precipitation decline and recent megadrought in central Chile. Geophys Res Lett 43(1):413–421

Boisier JP, Alvarez-Garretón C, Cordero RR et al (2018) Anthropogenic drying in central-southern Chile evidenced by long-term observations and climate model simulations. Elem Sci Anth 6(1)

Bonino G, Di Lorenzo E, Masina S, Iovino D (2019) Interannual to decadal variability within and across the major Eastern Boundary Upwelling Systems. Sci Rep 9(1):1–4

Camus P, Losada IJ, Izaguirre C et al (2017) Statistical wave climate projections for coastal impact assessments. Earth's Future 5(9):918–933

Castilla JC (1988) Earthquake-caused coastal uplift and its effects on rocky intertidal kelp communities. Science 242(4877):440–443

CC-COP25 (2019). Propuesta de un Sistema Integrado de Observación del Océano Chileno (SIOOC), Santiago, Chile. Comité Científico COP25, Ministerio de Ciencias, Chile

Church JA, Clark PU, Cazenave A et al (2013) Sea level change. In: Stocker TF, Qin D, Plattner G-K et al (eds) Climate change 2013: the physical science basis. Contribution of Working Group I to the Fifth Assessment Report of the Intergovernmental Panel on Climate Change. Cambridge University Press, Cambridge

CIESIN (2013) Low elevation coastal zone (LECZ) urban-rural population and land area estimates, version 2. Palisades, NY: NASA socioeconomic data and applications center (SEDAC). Columbia University. https://doi.org/10.7927/H4MW2F2J. Accessed 25/12/2017

Clemente M (2001) La red española de medida y registro de oleaje (REMRO): Un proyecto en continuo desarrollo. *Ing. Civ*. 121, 117e126. Data available at http://www.puertos.es/es-es/oceanografia/Paginas/portus.aspx

Combes V, Di Lorenzo E, Gómez F et al (2009) Modeling interannual and decadal variability in the Humboldt current upwelling system. J Phys Oceanogr

Comte D, Eisenberg A, Lorca E, Pardo M, Ponce L, Saragoni R, Singh SK, Suárez G (1986) The 1985 central Chile earthquake: a repeat of previous great earthquakes in the region? Science. 233(4762):449–453

CR² (2019) Explorador climático. (CR)² Center For Climate and Resilience Research. http://explorador.cr2.cl/. Accessed 24/03/2019

Cubillos L, Núñez S, Arcos D (1998) Primary production required to sustain the Chilean pelagic fisheries. Investig Mar 26:83–96

Dasgupta S, Laplante B, Meisner C, Wheeler D, Yan J (2007) The impact of sea level rise on developing countries: a comparative analysis. The World Bank

Dee DP, Uppala SM, Simmons AJ et al (2011) The ERA-Interim reanalysis: configuration and performance of the data assimilation system. Q J R Meteorol Soc 137(656):553–597

Enfield DB, Allen JS (1980) On the structure and dynamics of monthly mean sea level anomalies along the Pacific coast of North and South America. J Phys Oceanogr 10(4):557–578

Falvey M, Garreaud RD (2009) Regional cooling in a warming world: recent temperature trends in the southeast Pacific and along the west coast of subtropical South America (1979–2006). J Geophys Res Atmos 114(D4)

Fan Y, Lin SJ, Griffies SM, Hemer M (2014) Simulated global swell and wind-sea climate and their responses to anthropogenic climate change at the end of the twenty-first century. J Clim 27:3516–3536

Farías M, Vargas G, Tassara A et al (2010) Land-level changes produced by the Mw 8.8 2010 Chilean earthquake. Science 329(5994):916–916

Farías L, Besoain V, García-Loyola S (2015) Presence of nitrous oxide hotspots in the coastal upwelling area off central Chile: an analysis of temporal variability based on ten years of a biogeochemical time series. Environ Res Lett 10(4):044017

Flores-Aqueveque V, Rojas M, Aguirre C, Arias PA, González C (2020) South Pacific Subtropical High from the late Holocene to the end of the 21st century: insights from climate proxies and general circulation models. Clim Past 16(1):79–99

Fuenzalida H (1982) Un país de extremos climáticos. In: García H (ed) Chile, Esencia y Evolución. Universidad de Chile, Santiago, pp 27–35

Fyfe JC (2003) Extratropical Southern Hemisphere cyclones: harbingers of climate change? J Clim 16(17):2802–2805

Fyfe JC, Boer GJ, Flato GM (1999) The Arctic and Antarctic Oscillations and their projected changes under global warming. Geophys Res Lett 26(11):1601–1604

García-Reyes M, Sydeman WJ, Schoeman DS, Rykaczewski RR, Black BA, Smit AJ, Bograd SJ (2015) Under pressure: climate change, upwelling, and eastern boundary upwelling ecosystems. Front Mar Sci 16(2):109

Garreaud R (2009) The Andes climate and weather. Adv Geosci 22:3–11

Garreaud R, Battisti DS (1999) Interannual (ENSO) and interdecadal (ENSO-like) variability in the Southern Hemisphere tropospheric circulation*. J Clim 12(7):2113–2123

Garreaud RD, Falvey M (2009) The coastal winds off western subtropical South America in future climate scenarios. Int J Climatol 29(4):543–554

Garreaud RD, Muñoz RC (2005) The low-level jet off the west coast of subtropical South America: structure and variability. Mon Weather Rev 133(8):2246–2261

Garreaud RD, Alvarez-Garreton C, Barichivich J et al (2017) The 2010-2015 megadrought in central Chile: impacts on regional hydroclimate and vegetation. Hydrol Earth Syst Sci 21(12)

Garreaud R, Boisier JP, Rondanelli R, Montecinos A, Sepúlveda H, Veloso-Águila D (2019) The Central Chile mega drought (2010–2018): A climate dynamics perspective. Int J Climatol:1–19

Giesecke A, Capera AG, Leschiutta I et al (2004) The CERESIS earthquake catalogue and database of the Andean region: background, characteristics and examples of use. Ann Geophys 47(2–3)

Gillett NP, Fyfe JC (2013) Annular mode changes in the CMIP5 simulations. Geophys Res Lett 40:1189–1193

Gillett NP, Fyfe JC, Parker DE (2013) Attribution of observed sea level pressure trends to greenhouse gas, aerosol, and ozone changes. Geophys Res Lett 40:2302–2306

Gregg WW, Casey NW, McClain CR (2005) Recent trends in global ocean chlorophyll. Geophys Res Lett 32(3)

Hamilton G (1980) NOAA data buoy office programs. Bull Am Meteorol Soc 61(9):1012e1017 Data available at https://www.ndbc.noaa.gov/

Hemer MA, Church JA, Hunter JR (2010) Variability and trends in the directional wave climate of the Southern Hemisphere. Int J Climatol 30(4):475–491

Hu Y, Fu Q (2007) Observed poleward expansion of the Hadley circulation since 1979. Atmos Chem Phys 7(19):5229–5236

INE (2017) Estimaciones y Proyecciones de la Población de Chile 1992–2050 (Total País). www.censo2017.cl. Accessed 18/05/2019

INE (2018) Mapas Manzana – Entidad Censo 2017. Instituto Nacional de estadística. Disponible en http://ine-chile.maps.arcgis.com/apps/webappviewer/index.html?id=bc3cfbd4feec49699c11e813ae9a629f. Accessed 18/05/2019

IPCC (2019): Summary for policymakers. In: IPCC special report on the ocean and cryosphere in a changing climate. In press

Iriarte JL (2018) Natural and human influences on marine processes in Patagonian Subantarctic coastal waters. Front Mar Sci 8(5):360

Izaguirre C, Méndez FJ, Menéndez M, Losada IJ (2011) Global extreme wave height variability based on satellite data. Geophys Res Lett 38(10)

Lara C, Saldías GS, Tapia FJ et al (2016) Interannual variability in temporal patterns of chlorophyll–a and their potential influence on the supply of mussel larvae to inner waters in northern Patagonia (41–44 S). J Mar Syst 155:11–18

León-Muñoz J, Urbina MA, Garreaud R, Iriarte JL (2018) Hydroclimatic conditions trigger record harmful algal bloom in western Patagonia (summer 2016). Sci Rep 8:1330

Mann K, Lazier J (2006) Dynamics of marine ecosystems: biological-physical interactions in the oceans, Second edn. Blackwell Pub

Mantua NJ, Hare SR, Zhang Y, Wallace JM, Francis RC (1997) A Pacific interdecadal climate oscillation with impacts on salmon production. Bull Am Meteorol Soc 78(6):1069–1079

Martínez C, Contreras-López M, Winckler P, Hidalgo H, Godoy E, Agredano R (2018) Coastal erosion in central Chile: A new hazard? Ocean Coast Manag 156:141–155

Marrari M, Piola AR, Valla D (2017) Variability and 20-year trends in satellite-derived surface chlorophyll concentrations in large marine ecosystems around South and Western Central America. Front Mar Sci 4:372

Marshall GJ (2003) Trends in the Southern Annular Mode from observations and reanalyses. J Clim 16(24): 4134–4143

Masotti I, Aparicio-Rizzo P, Yevenes MA et al (2018) The influence of river discharge on nutrient export and phytoplankton biomass off the Central Chile coast (33°-37°S). Seasonal cycle and interannual variability. Front Mar Sci 5:423

McGranahan G, Balk D, Anderson B (2007) The rising tide: assessing the risks of climate change and human settlements in low elevation coastal zones. Environ Urban 19(1):17–37

Métois M, Socquet A, Vigny C et al (2013) Revisiting the North Chile seismic gap segmentation using GPS-derived interseismic coupling. Geophys J Int 194(3):1283–1294

Milne GA, Long AJ, Bassett SE (2005) Modelling Holocene relative sea-level observations from the Caribbean and South America. Quat Sci Rev 24(10–11):1183–1202

MMA (2019) Determinación del riesgo de los impactos del Cambio Climático en las costas de Chile, Report prepared by Winckler P, Contreras-López M, Vicuña S et al. Santiago, Chile

MMA (2020) Proceso de consulta pública del anteproyecto de ley marco de cambio climático. https://mma.gob.cl/proceso-de-consulta-publica-del-anteproyecto-de-ley-marco-de-cambio-climatico/

Montecino V, Lange CB (2009) The Humboldt Current System: ecosystem components and processes, fisheries, and sediment studies. Prog Oceanogr 83(1–4):65–79

Montecino HD, Ferreira VG, Cuevas A et al (2017) Vertical deformation and sea level changes in the coast of Chile by satellite altimetry and tide gauges. Int J Remote Sens 38(24):7551–7565

Montecinos A, Aceituno P (2003) Seasonality of the ENSO-related rainfall variability in central Chile and associated circulation anomalies. J Clim 16(2):281–296

Montecinos A, Purca S, Pizarro O (2003) Interannual-to-interdecadal sea surface temperature variability along the western coast of South America. Geophys Res Lett 30(11)

Muñoz R, Garreaud R (2005) Dynamics of the low-level jet off the West Coast of Subtropical South America. Mon Weather Rev 133:3661–3677

Newman M, Alexander MA, Ault TR, Cobb KM, Deser C, Di Lorenzo E, Mantua NJ, Miller AJ, Minobe S, Nakamura H, Schneider N (2016) The Pacific decadal oscillation, revisited. J Clim 29(12):4399–4427

Paris PJ, Walsh JP, Corbett DR (2016) Where the continent ends. Geophys Res Lett 43(23)

Pauly D, Zeller D (2016) Catch reconstructions reveal that global marine fisheries catches are higher than reported and declining. Nat Commun 7:10244

Perucca L, Alvarado P, Saez M (2016) Neotectonics and seismicity in southern Patagonia. Geol J 51(4):545–559

Pizarro O, Montecinos A (2004) Interdecadal variability of the thermocline along the west coast of South America. Geophys Res Lett 31(20)

Plafker G, Savage JC (1970) Mechanism of the Chilean earthquakes of May 21 and 22, 1960. Geol Soc Am Bull, 81(4), 1001–1030

Quiñones RA, Montes RM (2001) Relationship between freshwater input to the coastal zone and the historical landings of the benthic/demersal fish Eleginops maclovinus in central-south Chile. Fish Oceanogr, 10(4), 311–328

Rahn DA, Garreaud RD (2014) A synoptic climatology of the near-surface wind along the west coast of South America. Int J Climatol 34(3):780–792

Reguero BG, Losada IJ, Diaz-Simal P et al (2015) Effects of climate change on exposure to coastal flooding in Latin America and the Caribbean. PLoS One 10(7):e0133409

Renault L, Dewitte B, Falvey M, Garreaud R, Echevin V, Bonjean F (2009) Impact of atmospheric coastal jet off central Chile on sea surface temperature from satellite observations (2000–2007). J Geophys Res 114: C08006

Reyes O, Méndez C, San Román M, Francois JP (2018) Earthquakes and coastal archaeology: assessing shoreline shifts on the southernmost Pacific coast (Chonos Archipelago 43 50′–46 50′ S, Chile, South America). Quat Int 463:161–175

Saint-Amand P (1963) Special issue: oceanographic, geologic, and engineering studies of the Chilean earthquakes of May 1960. Bull Seismol Soc Am 53:1123–1436

Schneider W, Donoso D, Garcés-Vargas J, Escribano R (2017) Water-column cooling and sea surface salinity increase in the upwelling region off central-south Chile driven by a poleward displacement of the South Pacific High. Prog Oceanogr 151:38–48

Screen JA, Gillett NP, Stevens DP, Marshall GJ, Roscoe HK (2009) The role of eddies in the Southern Ocean temperature response to the Southern Annular Mode. J Clim 22(3):806–818

Semedo A, Suselj K, Rutgersson A, Sterl A (2011) A global view on the wind sea and swell climate and variability from ERA-40. J Clim 24:1461–1479

Sen PK (1968) Estimates of the regression coefficient based on Kendall's tau. J Am Stat Assoc 63(324):1379–1389

Seth A, Rauscher SA, Biasutti M et al (2013) CMIP5 projected changes in the annual cycle of precipitation in monsoon regions. J Clim 26(19):7328–7351

Simmonds I, Keay K (2000) Variability of southern hemisphere extratropical cyclone behavior, 1958–97. J Clim 13(3):550–561

Soto D, León-Muñoz J, Dresdner J, Luengo C, Tapia FJ, Garreaud R (2019 May) Salmon farming vulnerability to climate change in southern Chile: understanding the biophysical, socioeconomic and governance links. Rev Aquac 11(2):354–374

Strub PT, Mesías JM, Montecino V et al (1998) Coastal ocean circulation off western South America. In: Robinson AR, Brink KH (eds) The sea, vol 11. Wiley, pp 273–313

Strub PT, James C, Montecino V et al (2019) Ocean circulation along the southern Chile transition region (38°–46° S): mean, seasonal and interannual variability, with a focus on 2014–2016. Prog Oceanogr 172:159–198

Talley LD, Pickard G, Emery WJ, Swift JH (2011) Physical oceanography: an introduction. Elsevier Science and Technology, UK

Testa G, Masotti I, Farías L (2018) Temporal variability in net primary production in an upwelling area off central Chile (36 S). Front Mar Sci 5:179

Theil H (1950) A rank-invariant method of linear and polynomial regression analysis I, II, III. Nederl Akad Wetensch Proc 53:386–392, 521–525, 1397–1412

Thompson DW, Solomon S (2002) Interpretation of recent Southern Hemisphere climate change. Science 296(5569):895–899

Thompson DW, Wallace JM, Hegerl GC (2000) Annular modes in the extratropical circulation. Part II: trends. J Clim 13(5):1018–1036

UNISDR (2015) Global Risk Assessment GAR 2015: GVM and IAVCEI, UNEP, CIMNE and associates and INGENIAR, FEWS NET and CIMA Foundation

Wang D, Gouhier TC, Menge BA, Ganguly AR (2015) Intensification and spatial homogenization of coastal upwelling under climate change. Nature 518(7539):390

Wesson RL, Melnick D, Cisternas et al (2015) Vertical deformation through a complete seismic cycle at Isla Santa María, Chile. Nat Geosci 8(7):547–551

Wilcox R (2001) Fundamentals of modern statistical methods: substantially improving power and accuracy. Springer Science and Business Media

Young IR, Zieger S, Babanin SV (2011) Global trends in wind speed and wave height. Science 332:451

Zhang Y, Wallace JM, Battisti DS (1997) ENSO-like interdecadal variability. J Clim 10:1004–1020

**Publisher's note** Springer Nature remains neutral with regard to jurisdictional claims in published maps and institutional affiliations.

## Affiliations

**Patricio Winckler Grez** [1,2,3] **· Catalina Aguirre** [1,3,4] **· Laura Farías** [4,5] **· Manuel Contreras-López** [6] **· Ítalo Masotti** [3,4,7]

[1]   Escuela de Ingeniería Civil Oceánica, Universidad de Valparaíso, Valparaíso, Chile

[2]   Centro de Investigación y Gestión de Desastres Naturales (CIGIDEN-PUC), Santiago, Chile

[3]   Centro de Observación Marino para estudios de Riesgos del Ambiente Costero (COSTAR-UV), Valparaíso, Chile

[4]   Centro de Ciencia del Clima y la Resiliencia (CR2), Santiago, Chile

[5]   Departamento de Oceanografía, Universidad de Concepción, Concepción, Chile

[6]   Facultad de Ingeniería y Centro de Estudios Avanzados, Universidad de Playa Ancha, Valparaíso, Chile

[7]   Facultad de Ciencias del Mar y de Recursos Naturales, Universidad de Valparaíso, Valparaíso, Chile